The effective electroweak mixing angle $\sin^2\theta_{\text{eff}}$ with two-loop fermionic contributions

W. HOLLIK, U. MEIER and S. UCCIRATI

Max-Planck-Institut für Physik
(Werner-Heisenberg-Institut)
D-80805 München, Germany

Abstract

We present the results from a calculation of the full electroweak two-loop fermionic contributions to the effective leptonic mixing angle of the Z boson, $\sin^2\theta_{\text{eff}}$, in the Standard Model. On-shell renormalization and analytic calculations are performed for the three-point vertex functions at zero external momenta, whereas irreducible three-point integrals for non-vanishing external momenta are evaluated semi-analytically applying two different methods. Comparisons with a previous calculation show complete agreement.

1 Introduction

Precision observables at the Z-boson resonance, measured at LEP 1 and SLC, together with the masses of the W boson and of the top quark, measured at LEP 2 and the Tevatron, constitute a set of high-energy quantites which in comparison with the Standard Model predictions allow global precision analyses yielding indirect bounds on the Higgs-boson mass M_H [1]. In this context, one of the most important quantities with a very high sensitivity to M_H is the effective leptonic mixing angle, expressed as $\sin^2\theta_{\rm eff}$, in the effective couplings of the Z to leptons (electrons, to be precise). Besides M_W, it is a key observable measured with high experimental accuracy, with expected further improvements in the future. The current experimental value is 0.23147 ± 0.00017 [1]; a linear electron–positron collider with GigaZ capabilities could even reach an accuracy of 1.3×10^{-5} [2, 3]. Therefore, very precise and reliable theoretical predictions for $\sin^2\theta_{\rm eff}$ are required.

The electroweak mixing angle in the effective leptonic vertex of the Z boson can be defined via the relation (see e.g. [4])

$$\sin^2\theta_{\rm eff} \;\; = \;\; \frac{1}{4}\left(1 - {\rm Re}\,\frac{g_V}{g_A}\right), \tag{1}$$

in terms of the dressed vector and axial vector couplings $g_{V,A}$ in the Z–lepton vertex. Starting from the Z mass M_Z and the W mass M_W, $\sin^2\theta_{\rm eff}$ can be obtained in the following way,

$$\sin^2\theta_{\rm eff} \;\; = \;\; \kappa\, s_W^2 \;\; = \;\; \kappa\left(1 - \frac{M_W^2}{M_Z^2}\right), \quad \kappa = 1 + \Delta\kappa, \tag{2}$$

with higher-order contributions collected in the quantity $\Delta\kappa$. The W mass can be related to the precisely known Fermi constant G_F with the help of the W–Z interdependence,

$$M_W^2\left(1 - \frac{M_W^2}{M_Z^2}\right) \;\; = \;\; \frac{\pi\alpha}{\sqrt{2}G_F}(1 + \Delta r), \tag{3}$$

where Δr denotes the higher-order contributions. Recently, the full electroweak two-loop calculation for Δr has been completed, with both fermionic loops [5, 6] and purely bosonic loops [7], and further improvement by three-loop contributions to the ρ-parameter [8] and to the S parameter [9] has been given. Moreover, the universal QCD corrections via the self energies [10] are known.

For the κ factor in (2), fewer higher-order terms have been evaluated as yet. Besides the universal contributions through the ρ, S parameters and the QCD corrections, a top mass expansion for the electroweak two-loop corrections was performed [11], and only recently the complete two-loop electroweak corrections of the fermionic type, i.e. with at least one closed fermion loop, were calculated [12]. In this paper we present an independent calculation of those fermionic two-loop contributions and perform a comparison with the result of [12].

2 Electroweak two-loop contributions

Expanding the dressed couplings in (1) according to $g_{V,A} = g_{V,A}^{(0)} \left(1 + g_{V,A}^{(1)} + g_{V,A}^{(2)} + \cdots\right)$ in powers of α, one obtains the $O\left(\alpha^2\right)$ contribution to $\sin^2\theta_{\text{eff}}$ in the loop expansion

$$\sin^2\theta_{\text{eff}} \;=\; \sin^2\theta_{\text{eff}}^{(0)} + \sin^2\theta_{\text{eff}}^{(1)} + \sin^2\theta_{\text{eff}}^{(2)} + \mathcal{O}\left(\alpha^3\right) \tag{4}$$

to be

$$\sin^2\theta_{\text{eff}}^{(2)} \;=\; -\frac{g_V^{(0)}}{4g_A^{(0)}}\,\text{Re}\left(g_V^{(2)} - g_A^{(2)} + g_A^{(1)}\left(g_A^{(1)} - g_V^{(1)}\right)\right). \tag{5}$$

Hence, besides the two-loop diagrams depicted schematically in Fig. 1, products of one-loop contributions have to be taken into account. The circles in the diagrams of Fig. 1 denote the renormalized two- and three-point vertex functions, at the one-loop level in the reducible diagrams of Fig. 1a and 1b, and at two-loop order in the irreducible diagrams of Fig. 1c and 1d.

In our computation we have used the on-shell renormalization scheme as described in [5]. In this scheme the real part of the diagram shown in Fig. 1c vanishes. The reducible diagrams of Fig. 1a and 1b only contribute products of imaginary parts of one-loop functions, which can be easily computed. So the genuine two-loop task is the calculation of the irreducible $Z\ell\ell$-vertex diagrams in Fig. 1d.

For the computation of the two-loop corrections with at least one closed fermion loop we are directed to the vertex diagrams shown in Fig. 2, one-loop diagrams with one-loop counter term insertions of the fermionic type, and the two-loop fermionic counter term. In the combination entering (5), the two-loop counter term for $\sin^2\theta_{\text{eff}}$ in the on-shell scheme is given by

$$\delta\sin^2\theta_{\text{eff}}^{(2)} \;=\; \delta s_W^2 + \frac{1}{2s_W c_W}\delta Z_{(2)}^{\gamma Z} + s_W^2\left(s_W^2 - c_W^2\right)\delta Z_{(2)}^{\ell,L} - s_W^2\left(s_W^2 - c_W^2\right)\delta Z_{(2)}^{\ell,R} \tag{6}$$

$$+ \text{ products of one loop counter terms.}$$

$\delta Z_{(2)}^{\gamma Z}$ and $\delta Z_{(2)}^{\ell,L/R}$ are the field renormalization constants for the photon-Z two-point function and for the left-/right-handed lepton field. The counter term δs_W^2 for the on-shell quantity s_W^2 in (2) contains the two-loop counter terms for the Z- and W-boson masses, $\delta M_{Z/W(2)}^2$, and products of one-loop counter terms,

$$\delta s_W^2 \;=\; \frac{M_W^2}{M_Z^2}\left(\frac{\delta M_{Z(2)}^2}{M_Z^2} - \frac{\delta M_{W(2)}^2}{M_W^2}\right) - \frac{M_W^2}{M_Z^2}\frac{\delta M_{Z(1)}^2}{M_Z^2}\left(\frac{\delta M_{Z(1)}^2}{M_Z^2} - \frac{\delta M_{W(1)}^2}{M_W^2}\right). \tag{7}$$

Apart from the products of one-loop functions in (5) and the reducible diagram Fig. 1b only the two-loop counter term (6) yields contributions with two closed fermion loops.

The contributions with one closed fermion loop contain the generic two-loop diagrams depicted in Fig. 2. Their evaluation encounters a twofold task: the two-loop renormalization, and the computation of genuine two-loop vertex functions for non-vanishing external momenta. We have separated these two items by splitting the renormalized two-loop con-
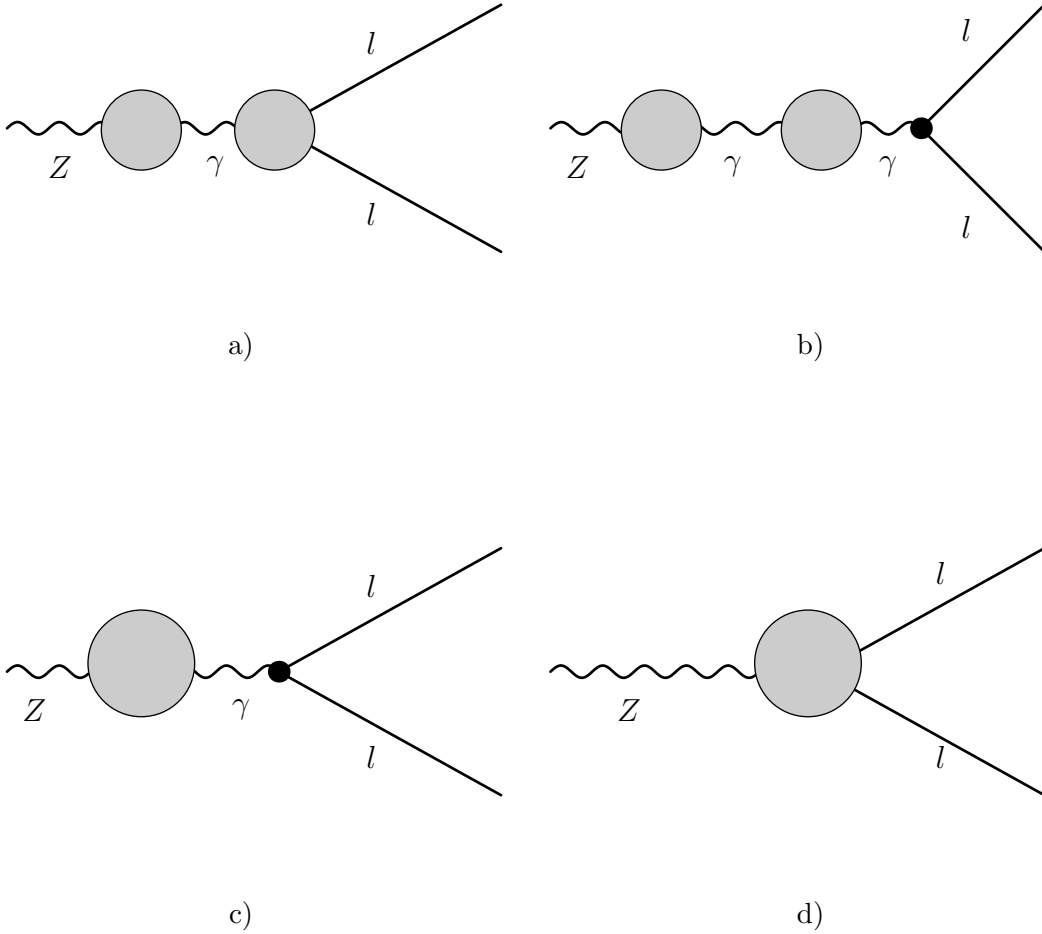

Figure 1: Classes of two loop diagrams

tribution to the $Z\ell\ell$ vertex function with the two external lepton momenta $p_\pm$,

$$\hat{\Gamma}_\mu^{Z\ell\ell\,(2)}(P^2) = \gamma_\mu\left(g_V^{(2)} - g_A^{(2)}\gamma_5\right), \qquad P^2 = (p_- + p_+)^2, \tag{8}$$

into two UV-finite pieces according to

$$\begin{aligned}
\hat{\Gamma}_\mu^{Z\ell\ell\,(2)}(M_Z^2) &= \Gamma_\mu^{Z\ell\ell\,(2)}(M_Z^2) + \Gamma_\mu^{CT} \\
&= \left[\Gamma_\mu^{Z\ell\ell\,(2)}(0) + \Gamma_\mu^{CT}\right] + \left[\Gamma_\mu^{Z\ell\ell\,(2)}(M_Z^2) - \Gamma_\mu^{Z\ell\ell\,(2)}(0)\right].
\end{aligned} \tag{9}$$

$\Gamma_\mu^{Z\ell\ell\,(2)}(P^2)$ denotes the corresponding unrenormalized $Z\ell\ell$ vertex, and Γ_μ^{CT} is the two-loop counter term, which is independent of P^2. The first term on the right hand side of (9) contains the complete two-loop renormalization, but no genuine two-loop vertex diagrams since in absence of external momenta they reduce to simpler vacuum integrals. All the genuine two-loop vertex diagrams appear as subtracted quantities in the second term on the right hand side of (9).
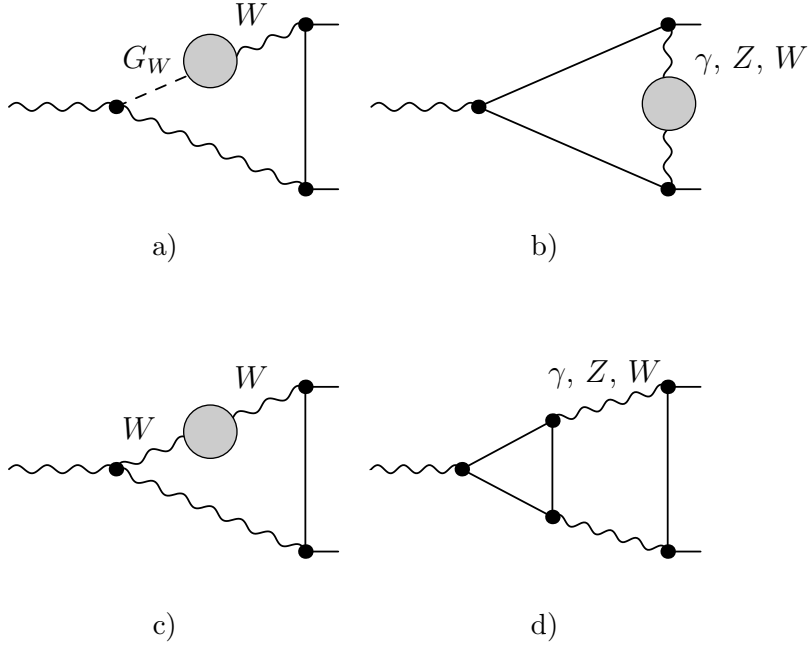

Figure 2: Irreducible two-loop vertex diagrams containing fermion loops.

4

3 Outline of the calculation

In order to calculate the irreducible vertex diagrams of Fig. 2, various techniques are applied. Diagrams containing a one-loop self-energy insertion are calculated with the help of dispersion relations. This results in one-dimensional integrals, which are computed numerically.

The diagrams with fermion triangles, Fig. 2d, require a careful treatment of γ_5 in D dimensions. In [5] it was shown that naive dimensional regularization with a four-dimensional treatment of the ϵ-tensor from traces involving γ_5 can be applied for this special case. Putting such traces to zero yields a UV-finite difference, which vanishes for a fermion generation with equal masses. Since the light fermion masses have been neglected in our approach, a non-vanishing contribution occurs only from the third generation. In the numerical discussion of section 4 this difference is labeled as the "γ_5" contribution.

Differently from the charged-current case treated in [5], the neutral-current vertex considered here involves another subtlety originating from photons in the internal lines of Fig. 2d, which give rise to collinear divergences in the case of massless electrons. This would produce unphysical finite extra shifts in combination with the $(D-4)$ terms from the γ_5 traces. [For massive internal bosons those terms disappear in the limit $D \to 4$ because the second loop integration does not introduce another UV divergence.] In order to prevent this kind of problems, we keep the physical mass of the external electrons in the dangerous diagrams. Moreover, also the masses of the internal b quarks and τ leptons have been kept. The resulting two-loop vertex functions are further evaluated using the methods described in [13]. In the end we are left with up to four-dimensional integrals, which are calculated numerically.

3.1 Computation of $\hat{\Gamma}_\mu^{Z\ell\ell\,(2)}(0)$

In order to get the renormalized vertex (respectively, the contribution to $\sin^2 \theta_{\text{eff}}$) from the two-loop vertex at zero momentum, the two-loop renormalization constants in (6) and (7) are needed. In the on-shell scheme [5] they are given by

$$\delta M_{W(2)}^2 = \text{Re}\left(\Sigma_{(2)}^W(M_W^2)\right) - \delta Z_{(1)}^W \delta M_{W(1)}^2 + \text{Im}\left(\Sigma_{(1)}^{W'}(M_W^2)\right) \text{Im}\left(\Sigma_{(1)}^W(M_W^2)\right), \quad (10)$$

$$\delta M_{Z(2)}^2 = \text{Re}\left(\Sigma_{(2)}^{ZZ}(M_Z^2)\right) - \delta Z_{(1)}^{ZZ} \delta M_{Z(1)}^2 + \text{Im}\left(\Sigma_{(1)}^{ZZ'}(M_Z^2)\right) \text{Im}\left(\Sigma_{(1)}^{ZZ}(M_Z^2)\right)$$

$$+ \frac{M_Z^2}{4}\left(\delta Z_{(1)}^{\gamma Z}\right)^2 + \frac{\text{Im}\left(\Sigma_{(1)}^{\gamma Z}(M_Z^2)\right)^2}{M_Z^2}, \quad (11)$$

$$\delta Z_{(2)}^{\gamma Z} = -2\frac{\text{Re}\left(\Sigma_{(2)}^{\gamma Z}(M_Z^2)\right)}{M_Z^2} + \delta Z_{(1)}^{Z\gamma}\frac{\delta M_{Z(1)}^2}{M_Z^2} - \frac{1}{2}\delta Z_{(1)}^{\gamma Z}\delta Z_{(1)}^{\gamma\gamma}, \quad (12)$$

involving the bosonic self energies and field renormalization constants, and

$$\delta Z_{(2)}^{\ell,L} = -\Sigma_{(2)}^{\ell,L}(0), \tag{13}$$

$$\delta Z_{(2)}^{\ell,R} = -\Sigma_{(2)}^{\ell,R}(0), \tag{14}$$

from the two-loop leptonic self energies according to the decomposition

$$\Sigma^{\ell}(p) = \not{p}\,\omega_L \Sigma^{\ell L}(p^2) + \not{p}\,\omega_R \Sigma^{\ell R}(p^2). \tag{15}$$

$\Sigma'(p^2)$ denotes the derivative of a self-energy $\Sigma(p^2)$ with respect to p^2.

The computation of the renormalized vertex at vanishing external momentum is done in the following steps. The Feynman diagrams are generated with the package *FeynArts* [14]. The program *TwoCalc* [15] is applied to reduce the amplitudes to standard integrals. The resulting scalar one-loop integrals and two-loop vacuum integrals are calculated using analytic results [16, 17]. The two-loop self-energy functions with non-vanishing external momenta appearing in the renormalization constants (10)-(12) are obtained with the help of one-dimensional integral representations [18].

3.2 Diagrams with self-energy insertions

The strategy to compute vertex diagrams with self-energy insertions for the subtracted vertex $\Gamma_\mu^{Z\ell\ell}(M_Z^2) - \Gamma_\mu^{Z\ell\ell}(0)$ will be illustrated in terms of Fig. 2b with a diagonal Z self-energy as an example (the other diagrams are calculated in an analogous way). The corresponding vertex diagram has the structure

$$\Gamma_\mu(P^2) \sim \int \mathrm{d}^D q \; \gamma^\rho (g_v - g_a \gamma_5) \frac{1}{\not{q} - \not{p}_-} \gamma_\mu (g_v - g_a \gamma_5) \frac{1}{\not{q} + \not{p}_+} \gamma^\sigma (g_v - g_a \gamma_5) \frac{\hat{\Sigma}_{\rho\sigma}(q)}{(q^2 - M_Z^2)^2}, \tag{16}$$

with $P^2 = (p_- + p_+)^2$. The renormalized one-loop self-energy can be decomposed into its transverse and longitudinal part,

$$\hat{\Sigma}_{\rho\sigma}(q) = \hat{\Sigma}_T(q^2)\left(g_{\rho\sigma} - \frac{q_\rho q_\sigma}{q^2}\right) + \hat{\Sigma}_L(q^2)\left(\frac{q_\rho q_\sigma}{q^2}\right). \tag{17}$$

It can be easily verified that for on-shell leptons the part proportional to $q_\rho q_\sigma$ yields a term independent of P^2, hence it drops out in the difference $\Gamma_\mu^{Z\ell\ell}(M_Z^2) - \Gamma_\mu^{Z\ell\ell}(0)$, and only the transverse part has to be taken into account. In the on-shell-scheme it reads

$$\hat{\Sigma}_T(q^2) = \Sigma_T(q^2) - \mathrm{Re}\,\Sigma_T(M_Z) - (q^2 - M_Z^2)\,\mathrm{Re}\,\Sigma_T'(M_Z^2) \tag{18}$$

$$= \Sigma_T(q^2) - \Sigma_T(M_Z^2) - (q^2 - M_Z^2)\,\Sigma_T'(M_Z^2)$$

$$+ i\,\mathrm{Im}\,\Sigma_T(M_Z^2) + i\,(q^2 - M_Z^2)\,\mathrm{Im}\,\Sigma_T'(M_Z^2).$$

Inserting the imaginary parts into (16), one gets a constant times one-loop functions. For the rest, we use the dispersion relation

$$\Sigma_T(q^2) = \frac{1}{\pi} \int_0^\infty \mathrm{d}s \, \frac{\mathrm{Im}\,\Sigma_T(s)}{s - q^2 - i\epsilon}, \tag{19}$$

6

yielding

$$\Sigma_T(q^2) - \Sigma_T(M_Z^2) - (q^2 - M_Z^2)\,\Sigma_T'(M_Z^2)$$

$$= -\frac{(q^2 - M_Z^2)^2}{\pi} \int_0^\infty \mathrm{d}s \, \frac{\mathrm{Im}\,\Sigma_T(s)}{(s - M_Z^2 - i\epsilon)^2} \frac{1}{(q^2 - s + i\epsilon)} \,. \tag{20}$$

Inserting this into (16), the factor $(q^2 - M_Z^2)^2$ cancels the corresponding term in the denominator, and we end up with a one-dimensional integral over a one-loop three-point function with one variable mass s, multiplied by the weight-factor $\mathrm{Im}\Sigma(s)/(s - M_Z^2)^2$. The subtraction at $P^2 = 0$ ensures that the expressions are UV finite. Finally we are left with integrals of the type

$$\int_0^\infty \mathrm{d}s \, \frac{f(s)}{(s - M^2 - i\epsilon)^2} = \int_0^{2M^2} \mathrm{d}s \, \frac{f(s) - f(M^2) - (s - M^2)f'(M^2)}{(s - M^2 - i\epsilon)^2} \tag{21}$$

$$+ \int_0^{2M^2} \mathrm{d}s \, \frac{f(M^2) + (s - M^2)f'(M^2)}{(s - M^2 - i\epsilon)^2}$$

$$+ \int_{2M^2}^\infty \mathrm{d}s \, \frac{f(s)}{(s - M^2)^2} \,.$$

The second term in (21) can be computed analytically. The other terms in (21) are free of singularities and can be integrated numerically. We have used the CUBA library [19] which allows a very fast and precise evaluation of the integrals.

3.3 Diagrams with fermion triangles

For the computation of the diagrams containing fermion triangles (Fig. 2d) we have basically adopted the numerical methods described in [13]. The mass of the external electron lines is set to zero except for the cases with internal $Z\,\gamma$ and $\gamma\,\gamma$, where m_e is used to regularize infrared and collinear divergences. In the cases $Z\,\gamma$ and $\gamma\,\gamma$ we have also kept all the internal fermion masses (b, t, τ), of the third generation, while in the cases $W\,W$ and $Z\,Z$ all fermions are treated as massless, except the top quark.

The resulting expression for the contribution to $\sin^2\theta_{\mathrm{eff}}^{(2)}$ in (1) can be written as a sum of terms from tensor integrals of the family V^{231} (the families of two-loop self-energies and vertices are collected in the appendix). In order to simplify as much as possible the tensorial structure, we perform a simple reduction of the type

$$\frac{2\,q \cdot p}{(q^2 + m^2)\,[(q + p)^2 + M^2]} = \frac{1}{q^2 + m^2} - \frac{1}{(q + p)^2 + M^2} - \frac{p^2 - m^2 + M^2}{(q^2 + m^2)\,[(q + p)^2 + M^2]},$$

which does not introduce any new denominator and therefore any spurious singularity. At this point we have a sum of tensor integrals up to rank 3 belonging to four vertex families $(V^{121}, V^{131}, V^{221}, V^{231})$, together with three self-energy types $(S^{111}, S^{121}, S^{131})$, and some one-loop diagrams (B and C functions).

For all these tensor integrals, Feynman parameters are introduced. The parameter integrals after integration over the loop momenta are manipulated in order to obtain smooth integrands to be computed numerically. The methods used are those described in [13] together with some improvement aimed to increase the numerical stability in specific regions of the phase-space (some new methods have been also developped for internal checks). In this context, it is worth mentioning the discovery of a new kind of algorithm for the computation of one-loop diagrams, which has been presented in [20]. The basic idea is that, given a polynomial V in the Feynman parameters $x = (x_1, x_2, \ldots)^t$, a constant B and a column vector $\mathcal{P}$ with

$$V(x) = Q(x) + B, \qquad \mathcal{P}^t \, \partial_x \, Q(x) = -Q(x), \tag{22}$$

it can be easily proved that the following relation holds $(\beta > 0)$,

$$\int \mathrm{d}x \, V(x)^\mu = \int \mathrm{d}x \, \left(\beta - \mathcal{P}^t \, \partial_x\right) \int_0^1 \mathrm{d}y \, y^{\beta-1} \, [Q(x) \, y + B]^\mu \, . \tag{23}$$

Since any one-loop diagram can be expressed as an integral of a quadratic polynomial to a negative power, the previous formula can be applied with $\mu < 0$. After an integration by parts, which cancels ∂_x, we can perform the integration in y. Then the procedure can be iterated with appropriate values of β to obtain smooth integrals. For example, for the scalar one-loop three-point function we obtain $(\varepsilon = 4 - D)$

$$C_0 = \left(\frac{\mu^2}{\pi}\right)^{\varepsilon/2} \Gamma\left(1 + \frac{\varepsilon}{2}\right) \int_0^1 dx_1 \int_0^{x_1} dx_2 \, V(x_1, x_2)^{-1-\varepsilon/2}.$$

$$= \sum_{i=0}^2 \frac{a_i}{2} \int_0^1 dx_1 \frac{1}{V[i](x_1) - B} \ln \frac{V[i](x_1)}{B} + \mathcal{O}(\varepsilon), \tag{24}$$

where

$$V(x) = x^t \, H \, x + 2 \, K^t \, x + L, \qquad B = L - K^t \, H^{-1} \, K, \qquad X = -H^{-1} \, K,$$
$$V[0](x_1) = V(1, x_1), \qquad V[1](x_1) = V(x_1, x_1), \qquad V[2](x_1) = V(x_1, 0),$$
$$a_0 = 1 - X_1, \qquad a_1 = X_1 - X_2, \qquad a_2 = X_2, \qquad X = (X_1, X_2)^t \, . \tag{25}$$

The matrix H, the column K, and the constant L are related to the physical quantities in the vertex diagram [Fig. 3] as follows $(j, l = 1, 2)$,

$$H_{lj} = -p_l \cdot p_j, \qquad K_j = \frac{1}{2}(k_j^2 - k_{j-1}^2 + m_{j+1}^2 - m_j^2), \qquad L = m_1^2 - i\epsilon,$$
$$k_0 = 0, \qquad k_1 = p_1, \qquad k_2 = p_1 + p_2 \, . \tag{26}$$

This representation for C_0 (which can be easily generalised for tensor integrals) is used to compute those two-loop diagrams that can be expressed as an integral of a one-loop three-point function, as in V^{221} and V^{231} (see [13] for explicit expressions). In such cases
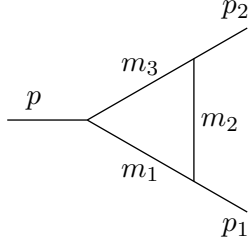
8

Figure 3: One-loop three-point function. The momenta are understood as incoming.

the masses and momenta of the C functions depend on Feynman parameters, which have to be integrated over. It is therefore crucial that the zeros of the denominator $(V[i](x_1) - B)$ in (24) are compensated by the logarithm.

Another important feature of the calculation is the infrared problem. Although the diagrams of Fig. 2d are IR finite, some individual integrals arising from the reduction in the $Z\gamma$ case are divergent. A typical case is the scalar part of the following diagram, which has the structure

For all the IR divergent integrals in the decomposition we have extracted the infrared one-loop functions and verified analytically that the sum of them cancels. The remaining finite terms are then again expressed in terms of smooth integrals and computed numerically. Details of this treatment of IR divergences will be given elsewhere [21].

The algebraic handling and the numerical evaluation has been done in parallel by two independent computations. For the numerical integration the NAG library D01GDF [22] was used in one case and the CUBA library [19] in the other one. According to the features of the integrator, the contribution to the final result are summed up either in a single integral or split into a sum of several terms. In the second case the total error has been computed as the sum of the errors of the different integrals. Thanks to the use of more than one method for each diagram type, it has been possible to achieve a good numerical precision and make a severe cross-check of the calculations.

9

4 Results

The input parameters for the evaluation of the final result are put together in Tab. 1. They are chosen in accordance with [12] in order to make an immediate comparison possible. M_W and M_Z are the experimental values of the W- and Z-boson masses [23], which are the on-shell masses. They have to be converted to the values in the pole mass scheme [5], labeled as $\overline{M}_W$ and $\overline{M}_Z$, which are used internally for the calculation. These quantities are related via $M_{W,Z} = \overline{M}_{W,Z} + \Gamma^2_{W,Z}/(2\,M_{W,Z})$. For Γ_Z the experimental value (Tab. 1) and for Γ_W the theoretical value has been used, *i.e.* $\Gamma_W = 3\,G_\mu M_W^3 / \left(2\sqrt{2}\pi\right) \left(1 + 2\alpha_s\left(M_W^2\right)/(3\pi)\right)$ with sufficient accuracy.

parameter	value
M_W	80.426 GeV
M_Z	91.1876 GeV
Γ_Z	2.4952 GeV
m_t	178.0 GeV
$\Delta\alpha\left(M_Z^2\right)$	0.05907
$\alpha_s\left(M_Z^2\right)$	0.117
G_μ	1.16637×10^{-5}
$\overline{M}_W$	80.3986 GeV
$\overline{M}_Z$	91.1535 GeV

Table 1: Input parameters entering our computation. M_W and M_Z are the experimental values of the W- and Z-boson masses, whereas $\overline{M}_W$ and $\overline{M}_Z$ are the calculated quantities in the pole mass scheme.

The results are given for $\Delta\kappa$, eq. (2), and are listed in Tab. 2 and Tab. 3 for various masses of the Higgs boson. Tab. 2 contains also the one-loop result for comparison and the corresponding results obtained in [12]. A finite b-quark mass has been kept in the one-loop result. The errors on our two-loop-results (in brackets) are due to the uncertainty from the numerical integration. Our results are in full agreement with those given in [12] (last column of Tab. 2).

In Tab. 3 the various parts of the two-loop result are shown. Large cancellations between the part containing two fermion loops and the part containing only one fermion loop occur. Moreover, one can see that, depending on the value of M_H, the first term of (9) (column 4) is about 15-20 times larger than the second one (column 5). Hence, the complete result for the renormalized $Z\ell\ell$ vertex at $P^2 = M_Z^2$ can be well approximated by the much simpler expression at $P^2 = 0$. The "γ_5" part is also very well approximated by its value at $P^2 = 0$, which is 0.280×10^{-4}. The "γ_5" part does not contain any terms proportional to m_t^4 or m_t^2; for illustration it is plotted in Fig. 4, at $P^2 = 0$ as a function of the top mass.

$M_H\,[GeV]$	$\mathcal{O}\left(\alpha\right)\times10^{-4}$	$\mathcal{O}\left(\alpha^2\right)\times10^{-4}$	$\mathcal{O}\left(\alpha^2\right)\times10^{-4}[12]$
100	438.937	-0.637(1)	-0.63
200	419.599	-2.165(1)	-2.16
600	379.560	-5.012(1)	-5.01
1000	358.619	-4.737(1)	-4.73

Table 2: Two-loop result for $\Delta\kappa$ in comparison with the one-loop result and the result in [12].

M_H [GeV]	2 ferm. loops $\times10^{-4}$	red. $\times10^{-4}$	$\hat{\Gamma}\left(0\right)$ $\times10^{-4}$	$\Gamma\left(M_Z^2\right)-\Gamma\left(0\right)$ $\times10^{-4}$	γ_5 $\times10^{-4}$
100	13.758	-0.722	-14.903	0.959(1)	0.271
200	13.758	-0.688	-16.465	0.959(1)	0.271
600	13.758	-0.501	-19.499	0.959(1)	0.271
1000	13.758	-0.386	-19.339	0.959(1)	0.271

Table 3: Breakdown of the two-loop result. The column "2 ferm. loops" gives all contributions with two closed fermion loops, whereas the other columns only contain results with one closed fermion loop. "red." refers to the reducible contribution of the diagrams depicted in Fig. 1a and Fig. 1b plus the product of one-loop contributions in (5). $\hat{\Gamma}\left(0\right)$ is the first term of (9) and $\Gamma\left(M_Z^2\right)-\Gamma\left(0\right)$ the second one. In the last column the "γ_5"-contributions are given (see text).
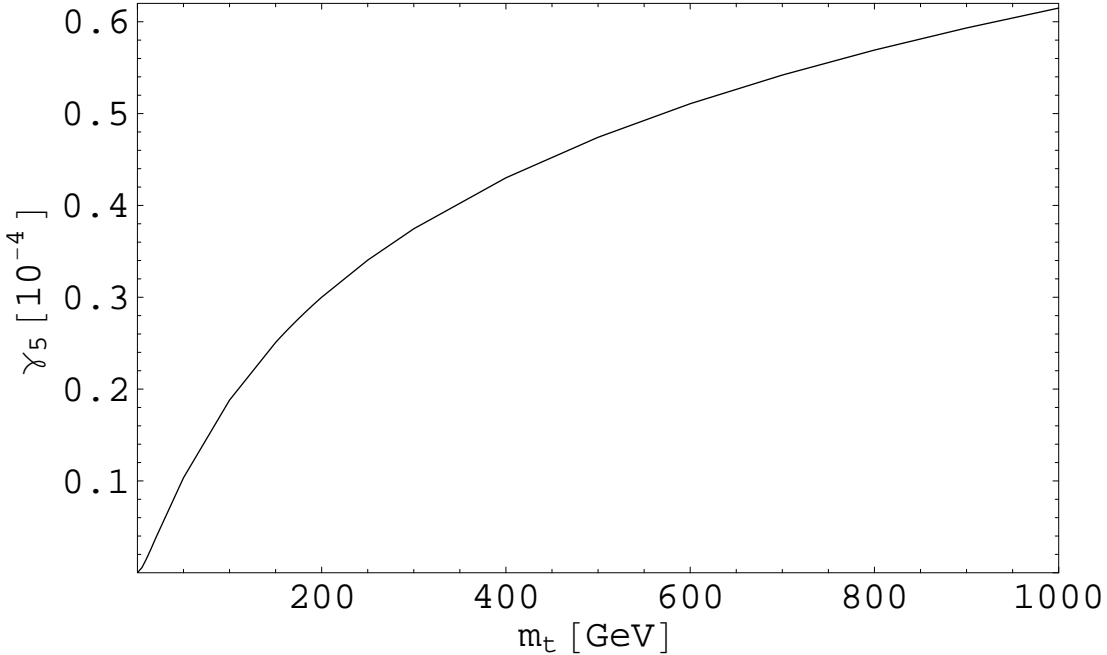

Figure 4: "γ_5" contribution at $P^2=0$ as a functions of m_t.

In conclusion, we have evaluated the electroweak 2-loop corrections to $\sin^2 \theta_{\text{eff}}$ with at least one closed fermion loop. Methods to calculate the appearing two-loop vertex functions have been described. A discussion of the various individual parts of the two-loop result was given and agreement with [12] was found.

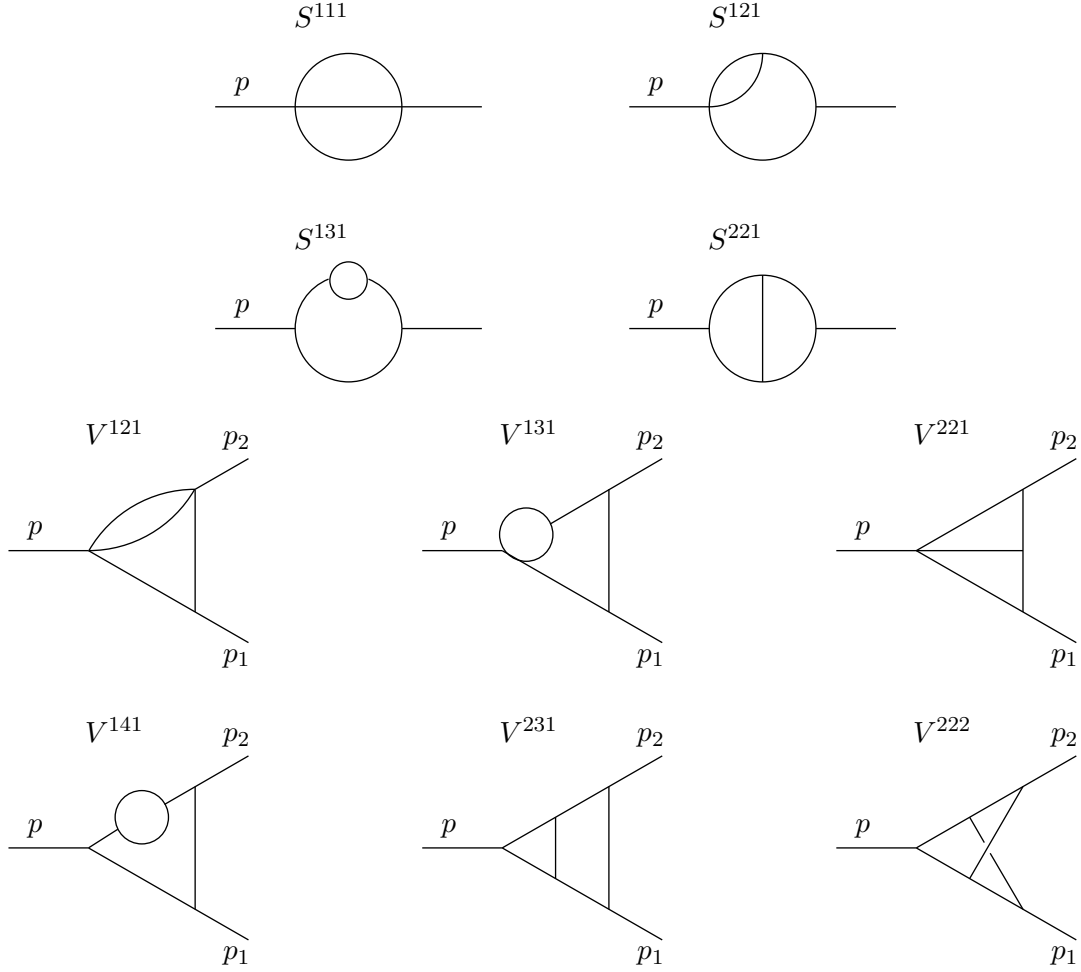# A   Two-loop self-energy and vertex families

Figure 5: Two-loop self-energy and vertex families. The momenta are all incoming and $p = -P = -(p_1 + p_2)$.

References

[1] The LEP Collaborations, the LEP Electroweak Working Group, the SLD Electroweak and Heavy Flavour Groups, arXiv:hep-ex/0412015.

[2] J. A. Aguilar-Saavedra *et al.*, TESLA Technical Design Report Part III: *Physics at an* e$^+$e$^-$ *Linear Collider* [hep-ph/0106315]. T. Abe *et al.* [American Linear Collider Working Group Collaboration], in *Proc. of the APS/DPF/DPB Summer Study on the Future of Particle Physics (Snowmass 2001)* ed. R. Davidson and C. Quigg, SLAC-R-570, *Resource book for Snowmass 2001* [hep-ex/0106055, hep-ex/0106056, hep-ex/0106057, hep-ex/0106058]. K. Abe *et al.* [ACFA Linear Collider Working Group Collaboration], ACFA Linear Collider Working Group report, [hep-ph/0109166].

[3] U. Baur, R. Clare, J. Erler, S. Heinemeyer, D. Wackeroth, G. Weiglein and D. R. Wood, in *Proc. of the APS/DPF/DPB Summer Study on the Future of Particle Physics (Snowmass 2001)* ed. N. Graf, eConf **C010630** (2001) P122 [arXiv:hep-ph/0111314].

[4] D. Y. Bardin *et al.*, hep-ph/9709229, in *Precision Calculations for the Z Resonance*, D. Bardin, W. Hollik, G. Passarino (Eds.), CERN 95-03.

[5] A. Freitas, W. Hollik, W. Walter and G. Weiglein, Phys. Lett. B **495** (2000) 338, E: ibid. B **570** (2003) 260 [hep-ph/0007091] and Nucl. Phys. B **632** (2002) 189, E: ibid. B **666** (2003) 305 [hep-ph/0202131].

[6] M. Awramik and M. Czakon, Phys. Lett. B **568**, 48 (2003) [hep-ph/0305248].

[7] M. Awramik and M. Czakon, Phys. Rev. Lett. **89** (2002) 241801 [hep-ph/0208113]. A. Onishchenko and O. Veretin, Phys. Lett. B **551** (2003) 111 [hep-ph/0209010]. M. Awramik, M. Czakon, A. Onishchenko and O. Veretin, Phys. Rev. D **68**, 053004 (2003) [hep-ph/0209084].

[8] J. van der Bij, K. Chetyrkin, M. Faisst, G. Jikia and T. Seidensticker, Phys. Lett. B **498** (2001) 156 [hep-ph/0011373]. M. Faisst, J. H. Kühn, T. Seidensticker and O. Veretin, Nucl. Phys. B **665**, 649 (2003) [hep-ph/0302275]. R. Boughezal, J.B. Tausk and J.J. van der Bij, Nucl. Phys. B **713**, 278 (2005) [hep-ph/0410216].

[9] R. Boughezal, J. B. Tausk and J. J. van der Bij, arXiv:hep-ph/0504092.

[10] A. Djouadi and C. Verzegnassi, Phys. Lett. B **195** (1987) 265; A. Djouadi, Nuovo Cim. A **100** (1988) 357; B. A. Kniehl, Nucl. Phys. B **347** (1990) 86; F. Halzen and B. A. Kniehl, Nucl. Phys. B **353** (1991) 567; B. A. Kniehl and A. Sirlin, Nucl. Phys. B **371** (1992) 141; A. Djouadi and P. Gambino, Phys. Rev. D **49** (1994) 3499 [Erratum-ibid. D **53** (1996) 4111] [arXiv:hep-ph/9309298]. K. G. Chetyrkin, J. H. Kühn and M. Steinhauser, Phys. Rev. Lett. **75** (1995) 3394 [arXiv:hep-ph/9504413], Nucl. Phys. B **482** (1996) 213 [arXiv:hep-ph/9606230].

[11] G. Degrassi, P. Gambino and A. Sirlin, Phys. Lett. B **394**, 188 (1997) [arXiv:hep-ph/9611363].

[12] M. Awramik, M. Czakon, A. Freitas and G. Weiglein, Phys. Rev. Lett. **93** (2004) 201805 [arXiv:hep-ph/0407317], Nucl. Phys. Proc. Suppl. **135** (2004) 119 [arXiv:hep-ph/0408207].

[13] A. Ferroglia, M. Passera, G. Passarino and S. Uccirati, Nucl. Phys. B **680** (2004) 199 [arXiv:hep-ph/0311186]; S. Actis, A. Ferroglia, G. Passarino, M. Passera and S. Uccirati, Nucl. Phys. B **703** (2004) 3 [arXiv:hep-ph/0402132]. G. Passarino, Nucl. Phys. B **619** (2001) 257 [arXiv:hep-ph/0108252]. G. Passarino and S. Uccirati, Nucl. Phys. B **629** (2002) 97 [arXiv:hep-ph/0112004].

[14] J. Küblbeck, M. Böhm and A. Denner, Comp. Phys. Comm. **60** (1990) 165. T. Hahn, Nucl. Phys. Proc. Suppl. **89** (2000) 231 [arXiv:hep-ph/0005029], Comput. Phys. Commun. **140** (2001) 418 [arXiv:hep-ph/0012260], *FeynArts User's Guide* and *LoopTools User's Guide*, available at http://www.feynarts.de.

[15] G. Weiglein, R. Scharf and M. Böhm, Nucl. Phys. B **416** (1994) 606 [arXiv:hep-ph/9310358]; G. Weiglein, R. Mertig, R. Scharf and M. Böhm, PRINT-95-128 *Prepared for 2nd International Workshop on Software Engineering, Artificial Intelligence and Expert Systems for High-energy and Nuclear Physics, La Londe Les Maures, France, 13-18 Jan 1992*

[16] G. 't Hooft and M. J. G. Veltman, Nucl. Phys. B **153** (1979) 365.

[17] A. I. Davydychev and J. B. Tausk, Nucl. Phys. B **397** (1993) 123.

[18] S. Bauberger, M. Böhm, G. Weiglein, F. A. Berends and M. Buza, Nucl. Phys. Proc. Suppl. **37B** (1994) 95 [arXiv:hep-ph/9406404]; S. Bauberger, F. A. Berends, M. Böhm and M. Buza, Nucl. Phys. B **434** (1995) 383 [arXiv:hep-ph/9409388]; S. Bauberger and M. Böhm, Nucl. Phys. B **445** (1995) 25 [arXiv:hep-ph/9501201].

[19] T. Hahn, arXiv:hep-ph/0404043.

[20] S. Uccirati, Acta Phys. Polon. B **35** (2004) 2573 [arXiv:hep-ph/0410332].

[21] G. Passarino and S. Uccirati, Two-Loop Vertices in Quantum Field Theory: Infrared Divergent Configurations, work in preparation.

[22] NAG Fortran Library, Mark 19, The Numerical Algorithms Group Ltd, Oxford UK. 1999.

[23] S. Eidelman et al. [Particle Data Group], Phys. Lett. B **592** (2004) 1.